Chapter 5

Geochemistry of the Ediacaran Browns Hole basalt, Utah: implications for the timing of western Laurentian rifting.

ABSTRACT

Trace element and U-Pb apatite data from the Ediacaran Browns Hole basalt in northern Utah, coupled with new regional correlations based on existing C isotope data from underlying strata, provide strong evidence that the basalt is rift-related and was erupted after deposition of Marinoan cap carbonates within the Cordilleran continental margin, providing some of the youngest geological evidence yet documented for the rifting of western Laurentia. Paleomagnetic data from the basalt and sedimentary rocks above and below it fail a fold test, indicating that the original magnetic orientation of these rocks was overprinted during or after Mesozoic to early Cenozoic folding.

INTRODUCTION

In the ~90 My following the last of the Snowball Earth events, the earth underwent some of the most remarkable changes in its history, including the radiation of multicellular organisms (e.g., Knoll and Carroll, 1999), the continued breakup of a supercontinent (e.g., Hoffman, 1991), the final stage in the oxidation of the oceans (Rothman et al., 2003), the largest negative C isotope excursion in earth history (e.g., Fike et al., 2006), an additional glaciation (Bowring et al., 2003), and possibly an episode of true polar wander (Kirschvink et al., 1997). Significant uncertainty surrounds the relative timing of these events and how they may relate to one another. The final stage in the rifting of western

Laurentia has been variously estimated at ca. 635 Ma based on geological evidence (e.g., Prave, 1999) and 550-600 Ma based on tectonic subsidence models (e.g., Bond et al, 1985). The Gaskiers glaciation, which followed what seem to be the more widespread Sturtian and Marinoan glaciations (i.e., the "Snowball Earth" events), has been radiometrically dated at 580 Ma (Bowring et al., 2003). Paleomagnetic data from the Sept. Iles intrusion in Quebec have been interpreted as indicative of an episode of inertial interchange true polar wander (IITPW) between 561 and 564 Ma (Kirschvink et al., 2005). Estimates for the onset of the Shuram anomaly C isotope excursion, which may have resulted from oxidation of a large reservoir of organic carbon (Fike et al., 2006), include before (Abolins et al., 2000, Halverson et al., 2007) and after (Condon et al., 2005, Fike et al., 2006) the Gaskiers glaciation, and available radiometric data constrain it only between ~551 and 600 Ma (Condon et al., 2005, Le Guerroué et al., 2006). Incision of km deep canyons into the syn-Shuram anomaly Wonoka Fm. of South Australia (e.g., Calver, 2000) may be related to sea-level drawdown resulting from the 580 Ma Gaskiers glaciation or ca. 560 Ma IITPW (Kirschvink et al., 2005).

Neoproterozoic strata in northern Utah, which include glacial diamictites (e.g., Ojakangas and Matsch, 1980) preserved in paleocanyons (Crittenden et al., 1978, Christie-Blick et al., 1989) and a basalt flow (Crittenden and Wallace, 1973) possibly related to the rifting of Laurentia, hold some promise for shedding light on this debate. Because these rocks are generally unmetamorphosed, they also have the potential for providing paleomagnetic data pertinent to discussions of late Precambrian true polar wander.

We collected samples of late Neoproterozoic strata from the Browns Hole quadrangle (Crittenden, 1972) just east of Huntsville, Utah (Fig. 1). Stratigraphic relationships and a new analysis of pre-existing C isotope data from the Ediacaran strata of northern Utah and southern Idaho in light of new chemostratigraphic data from the Death Valley region (Petterson et al., 2007) confirm that the Browns Hole basalt is younger than Marinoan cap carbonates. The Mineral Fork Tillite of northern Utah is almost certainly pre-Gaskiers in age based on our geochronology data from the basalt and the stratigraphic relationship between it and the tillite, a conclusion which is in agreement with regional stratigraphic studies (Crittenden et al., 1971, Crittenden et al., 1983).

NORTHERN UTAH NEOPROTEROZOIC-CAMBRIAN STRATIGRAPHY

Proterozoic strata in northern Utah and southern Idaho were part of a westward thickening wedge of rift-related and passive margin sediments (Stewart, 1970). East-vergent thrusting during the Mesozoic and Early Cenozoic disrupted the original distribution of sediments within this wedge such that the thickest, most basinal sections can now be found in the upper plates of regional thrust sheets and the most platformal sections are preserved within the autochthon (Crittenden et al., 1983). Our work is concentrated in the Browns Hole quadrangle which, except for a small area at the southern edge of the quadrangle, is situated in the hanging wall of the Willard-Paris thrust (Crittenden, 1972). Precambrian strata in this area include, in ascending order, the Maple Canyon Fm., Kelley Canyon Fm., Caddy Canyon Quartzite, Inkom Fm., Mutual Fm., and Browns Hole Fm. Above these units is the Precambrian(?) to Cambrian Geersten Canyon Quartzite (Fig. 2). The Precambrian-Cambrian boundary has not been

definitively located within this section, but *Skolithos* burrows have been found at the top of the Geersten Canyon Quartzite (Crittenden et al., 1971). These Neoproterozoic through Cambrian strata are predominantly sandstones and siltstones; the only mapped carbonates are thin layers in the Kelley Canyon Fm. These units and overlying Paleozoic sediments are folded into a NNE- plunging anticline in the Browns Hole quadrangle and are unconformably overlain by Upper Cretaceous to Paleogene conglomerates (Fig. 3, Crittenden, 1972).

Our study is focused on the interval from the Inkom Fm. to the Geersten Canyon Quartzite. The Inkom Fm. is comprised almost entirely of siltstone and is about 120 to 150m thick within the quadrangle (Crittenden, 1972). Disconformably overlying it are coarse-grained sandstones of the Mutual Fm., which range from approximately 150 to 400m in thickness across the area. The volcanic member of the Browns Hole Fm. conformably overlies the Mutual Fm. (Christie-Blick and Levy, 1989) and consists of ~60 to 150m of volcanic breccia, basalt, and sandstone. Above this is the Terra cotta quartzite member of the Browns Hole Fm., made up of roughly 30 to 50m of cross-bedded sandstone with frosted quartz grains and wind ripples that has been interpreted as an eolian or very shallow water deposit (Crittenden et al., 1971, Christie-Blick et al., 1989). Disconformably overlying the Browns Hole Fm. are ~400m of sandstone comprising the lower member of the Geersten Canyon Quartzite.

To the northwest of Huntsville, and also in the hanging wall of the Willard-Paris thrust, the Maple Canyon Fm. overlies the formation of Perry Canyon (Sorensen and Crittenden,

1976, and Crittenden et al., 1983), which contains two diamictites separated by siltstone, greywacke, and limestone. The lower diamictite unconformably overlies rocks of presumed Paleoproterozoic age, varies from 0 to 365m in thickness, and contains metavolcanic rocks near its base (Crittenden et al., 1983).

To the south in Big Cottonwood Canyon (Fig. 1), the Mutual Fm. disconformably overlies the Mineral Fork Tillite, which is filling a canyon eroded into the underlying Big Cottonwood Fm (Crittenden et al., 1978). Although the Browns Hole basalt is absent in this section, stratigraphic relationships indicate that it is younger than the Mineral Fork Tillite. The previous age determined for the basalt of 580±16 Ma (2σ) (discussed in detail below) thus leaves open the possibility that the tillite is Gaskiers in age. However, this location is within the autochthon and is one of the thinnest exposures of Neoproterozoic glacial stratigraphy in the region (Crittenden et al., 1983). Previous work has concluded that the Mutual Fm. disconformably overlies the tillite (Crittenden et al., 1983) implying that significant time may have elapsed between glaciation and deposition of the Mutual Fm.

ANALYTICAL DATA

Trace element data, Browns Hole basalt

Major and trace element data were obtained for a sample of the Browns Hole basalt using X-ray fluorescence (XRF) at the Ronald B. Gilmore XRF laboratory at the University of Massachusetts (Table 1). Details of the analytical procedure can be found in Rhodes (1996). The basalt is porphyritic and consists of clinopyroxene and plagioclase

phenocrysts in a groundmass of plagioclase. It contains 43.5 wt.% SiO_2, 6.09 wt.% MgO, 38 ppm Ni, and 33 ppm Cr, and has an olivine-diopside-nepheline normative assemblage. Relatively low Cr and Ni contents, as well as the absence of olivine phenocrysts, suggest that the basalt has probably undergone some degree of assimilation and fractional crystallization. On a total alkali-silica diagram it plots in the tephrite/basanite field (Fig. 4A), and because it contains >10 wt.% normative olivine it is classified as a basanite (Le Maitre et al., 1989). Although technically not a basalt, the term "Browns Hole basalt" is established in the literature, and we use the term "basalt" throughout this paper for the sake of clarity.

As illustrated on a MORB-normalized trace element diagram (Fig. 4B), the basalt is strongly enriched in the most incompatible trace elements, particularly Rb and Ba. As expected, the data provide no indication of a subduction zone environment, e.g. there is no Nb-depletion, the most common characteristic of arc volcanism (Gill, 1981). Continental basalts with enriched incompatible element concentrations relative to mid-ocean ridge basalts are frequently ascribed to low degrees of partial melting accompanying rifting (e.g., Fitton and Dunlop, 1985). Trace element compositions of the Browns Hole basalt are quite reminiscent of significantly older basalts within the formation of Perry Canyon and equivalent units in northern Utah and southern Idaho that are associated with earlier phases of the break-up of Rodinia (Harper and Link, 1986).

Geochronology

The Browns Hole basalt is one of the few Ediacaran volcanic units in North America, and its age is therefore of considerable interest. Crittenden and Wallace (1973) obtained an $^{40}Ar/^{39}Ar$ hornblende total gas age of 570±7 Ma (1σ) from a clast within volcanic breccia underlying the Browns Hole basalt. This age was subsequently re-calculated to 580±8 Ma (1σ) using new Ar decay constants (Christie-Blick and Levy, 1989). Because of uncertainties in the validity of this age, including the fact that the date was obtained from a clast underlying the basalt flow and not the flow itself, we collected new samples of the basalt to attempt a modern geochronological study. We recovered no zircon or baddeleyite, but apatite is relatively common within the basalt. U-Pb ages were determined on apatite grains using the isotope dilution thermal ionization mass spectrometry (ID-TIMS) method in the geochronology laboratory at the Massachusetts Institute of Technology. Because of low U concentrations (<2 ppm) within these apatites, the U-Pb age is very sensitive to the common-Pb correction, making it useless to rely on modeled initial Pb ratios such as those from Stacey and Kramers (1975). In order to precisely estimate the initial common-Pb of apatite, we step-leached Pb from ~75 hand-picked plagioclase grains using a method modified from Housh and Bowring (1991) and determined isotopic ratios of this nonradiogenic Pb. Our best estimate for the age of the apatites thus determined is the weighted mean $^{206}Pb/^{238}U$ age of two multi-grain analyses, which is 609±25 Ma (2σ) (Fig. 5, Table 2). However, one of these analyses is slightly discordant, and both multi-grain fractions may be on a mixing line defined by two single-grain analyses, one concordant and one discordant, in which case

the actual age may be older. In either case, it would seem that the previous radiometric date of 580±16 Ma (2σ) is a slight underestimate of the age of the basalt.

Paleomagnetic data

We collected 33 oriented block samples from the Inkom Fm. through the lower Geersten Canyon Quartzite (Fig.2) in the Browns Hole quadrangle. In order to conduct a paleomagnetic fold test, samples were collected from both the north and south limbs of the plunging anticline in the quadrangle (Fig. 3). Following measurements of natural remanent magnetization (NRM), each sample was cooled in LN_2 to unlock multi-domain magnetite and then underwent alternating field demagnetization to 10 mT followed by about 15 to 30 thermal demagnetization steps from 60 to ~680°C.

Paleomagnetic directions were determined from principal component analysis of these demagnetization data (Kirschvink, 1980) and primarily reveal two magnetization components (Fig. 6). The low temperature component, which is present in almost all of the samples, has an orientation close to that of the present-local magnetic field (PLF, Fig. 6A and B). Removal of this component with AF and relatively low temperature thermal demagnetization reveals a higher temperature component in many of the samples that we have denoted the B component. It is present in all of the basalt samples (Fig. 6C) and in many from the overlying and underlying sediments (Fig. 6D). When plotted in geographic (i.e., in situ, or non tilt-corrected) coordinates, the orientations of B components from samples from the north and south limbs of the fold overlap (Fig. 6E). When plotted in tilt-corrected coordinates, however, orientations of samples from the two

limbs clearly fall into different groups according to the limb from which they were collected (Fig. 6F). It is clear that this component fails a fold-test, i.e., the B component magnetization was acquired during or after folding and is thus not the primary remanence of the samples.

In a few (~5) of the samples there appears to be an additional, still higher temperature component. Orientations of this component are uniformly low-inclination (Fig 6 G and H), but declinations are scattered. Because of the scatter in declination and the limited number of samples with evidence for this component, a fold test is inconclusive. The low-inclination component is present in some of the sedimentary rocks but not in any samples from the basalt, suggesting that it is carried only by hematite (Curie temperature≈675°C), which is present in many of the sandstones, and has been completely overprinted in magnetite (Curie temperature=578°C), which is the overwhelming ferromagnetic mineral in the basalt. It is very doubtful that strata of the Huntsville area ever reached temperatures this high (which probably would have reset the hornblende $^{40}Ar/^{39}Ar$ age from the volcanic clast), but chemical alteration could have overprinted the primary magnetic orientation at much lower temperature. Of the 5 samples in which we observe the low-inclination component, four are from the Mutual Fm. and the other is from the Terra cotta quartzite member of the Browns Hole Fm., so any future paleomagnetic studies of the area should probably focus on these units.

DISCUSSION

Correlations with Death Valley

Although Neoproterozoic through Cambrian strata in northern Utah and southern Idaho are predominantly siliciclastic, C isotope compositions have previously been measured for many of the carbonate beds that are present. $\delta^{13}C_{carb}$ data are available for the Scout Mountain member of the Pocatello Fm. (Smith et al., 1994, Lorentz et al., 2004), the Blackrock Canyon Limestone (Smith et al., 1994, Corsetti et al., 2007), and carbonates within the Caddy Canyon Quartzite (Smith et al., 1994). As explained below, although these analyses are limited, it is nevertheless possible to confidently correlate these strata with equivalent units in the Death Valley region through a combination of lithologic similarities and C isotope chemostratigraphy. Our conclusions differ significantly from previous comparisons between the northern Utah/southern Idaho and Death Valley Neoproterozoic sections (e.g., Corsetti et al., 2007) and are made possible by new lithostratigraphic and C isotope data from the Noonday Dolomite (Petterson et al., 2007).

Corsetti et al. (2007) noted that carbonates overlying the upper of two diamictites in the Scout Mt. member of the Pocatello Fm. are lithologically quite similar to the Ibex Fm. in the Death Valley region (Corsetti and Kaufman, 2005), which, based on the work of Petterson et al. (2007) is equivalent to the Sentinel Peak and Radcliff members of the Noonday Dolomite. $\delta^{13}C_{carb}$ from carbonates immediately above diamictite in the Pocatello Fm. are about -3.0 to -3.5‰ (Fig. 7, Smith et al., 1994), values which are nearly identical to previously determined $\delta^{13}C_{carb}$ for the Sentinel Peak and lower Radcliff members of the Noonday Dolomite (Corsetti and Kaufman, 2005, Petterson et al., 2007).

~100m above these carbonates in the Pocatello Fm. are an additional ~25m of carbonate with $\delta^{13}C$ values ranging from about -4 to -6‰ (Smith et al., 1994, Lorentz et al., 2004), identical to values from the lower Radcliff member (Petterson et al., 2007). Based on these lithological and chemical similarities, we suggest that these lower and upper carbonates overlying diamictite in the Scout Mt. member are equivalent to the Sentinel Peak and Radcliff members, respectively, of the Noonday Dolomite.

C isotope values from the Middle Carbonate member of the Caddy Canyon Quartzite range from 3.9 to 8.8‰ (Smith et al., 1994), some of the heaviest values reported from Cordilleran Neoproterozoic carbonates. Corsetti et al. (2007) suggest that these beds are equivalent with the middle Johnnie Fm. in the Death Valley area, but the heaviest C isotope values from the Johnnie Fm. are only 3.3‰ (Corsetti and Kaufman, 2003). Current compilations of Neoproterozoic C isotope data (Halverson et al. 2005) indicate that $\delta^{13}C$ values became as heavy as 8.8‰ at only one point in the Ediacaran Period, at a time corresponding with deposition of the Mahogany Flats member of the upper Noonday Dolomite (Petterson et al., 2007). Based on this observation we suggest that the Middle Carbonate member of the Caddy Canyon Quartzite correlates with the upper Noonday Dolomite. C isotope values from the Blackrock Canyon Limestone, situated between the Pocatello Formation and Caddy Canyon Quartzite and correlated with carbonates in the Kelley Canyon Fm. by Crittenden et al. (1971), are generally -1.5 to 0‰ in the lower part and about 0 to 1‰ in the upper part (Fig. 7, Smith et al., 1994, Corsetti et al., 2007). Although these values are not unique to any particular time, they are consistent with data from the middle to upper part of the Noonday Dolomite (Petterson et al., 2007).

We thus conclude from pre-existing C isotope data that the Noonday Dolomite is equivalent to strata ranging from carbonates in the upper part of the Scout Mt. member of the Pocatello Fm. through at least the Middle Carbonate member of the Caddy Canyon Quartzite (Fig. 7). By this interpretation, Scout Mt. member carbonate overlying the younger of two diamictites in the Pocatello Fm. are cap dolostones, and the interval above this, to at least the Middle Carbonate member of the Caddy Canyon Quartzite, if not to the contact with the Upper Fluvial member, is a "cap-carbonate sequence" as defined by Hoffman and Schrag (2002). If this interpretation is correct, it would suggest that the Shuram anomaly is present somewhere in overlying strata below the *Skolithos*-bearing beds in the upper part of the Camelback Mt. Quartzite. Unfortunately, carbonates beds are rare to completely absent in this interval and C isotope data are unavailable. Christie-Blick and Levy (1989) correlated the contact between the Inkom and Mutual Fms. with a sequence boundary at the Johnnie Fm.-Stirling Quartzite contact in the Death Valley region. If this correlation is valid, it would suggest that the Shuram anomaly is present within the Inkom Fm., unless it has been removed by erosion as it almost was in sections of the Johnnie Fm. to the southeast of Death Valley (Chapter 4). In terms of lithostratigraphy, this is the most obvious correlation: the contact between Inkom Fm. siltstones and overlying Mutual Fm. sandstones is lithologically quite reminiscent of the contact between Johnnie Fm. siltstones and overlying Stirling Quartzite sandstones, and the unconformity within the upper part of the Caddy Canyon Quartzite may correlate with karst developed at the Johnnie-Noonday contact (Summa, 1993). However, the Shuram anomaly can be no older than ~600 Ma. based on U-Pb dates from detrital

zircons near the base of the anomaly in Oman (Le Guerroué et al., 2006). Given our best estimate for the age of the Browns Hole basalt (609±25 Ma), it is unlikely that the Inkom Fm., located at least 150m below the basalt and separated from it by what may be a significant unconformity at the base of the Mutual Fm., could be as young as 600 Ma, although we cannot entirely rule out this possibility because of the large uncertainties associated with the apatite U-Pb age. This reasoning would suggest, however, that the Shuram anomaly corresponds with some part of the Mutual Fm., Browns Hole Fm., and/or lower part of the Geersten Canyon Quartzite, or has been removed along an unconformity within this interval.

CONCLUSIONS

Regardless of the exact position of the Shuram anomaly, if our correlation of carbonates in the Caddy Canyon Quartzite with the upper Noonday Dolomite is correct, it implies that the Browns Hole basalt is distinctly post-Noonday. Coupled with trace element data which indicate that the basalt is probably related to extension, this observation suggests that in at least one place, the rifting of western Laurentia continued later than estimated by most geological studies (e.g., Prave, 1999), a conclusion which is consistent with the results from tectonic subsidence models (e.g., Bond et al., 1985). U-Pb data from the basalt indicate that it is older than proposed latest Proterozoic (ca. 560 Ma) IITPW (Kirschvink et al., 2005).

REFERENCES

Abolins, M., Oskin, R., Prave, T., Summa, C., and Corsetti, F., 2000, Neoproterozoic glacial record in the Death Valley region, California and Nevada, *in* Lageson, D.R., Peters, S.G., and Lahren, M.M., eds., Great Basin and Sierra Nevada: Boulder, Geological Society of America Field Guide 2, p.319-335.

Bond, G.C., Christie-Blick, N., Kominz, M.A., and Devlin, W.J., 1985, An early Cambrian rift to post-rift transition in the Cordillera of western North America, v. 315, p. 742-746.

Bowring, S.A., Myrow, P.M., Landing, E., Ramezani, J., and Grotzinger, J.P., 2003, Geochronological constraints on terminal Neoproterozoic events and the and the rise of metazoans: Geophysical Research Abstracts, 5, 13219.

Calver, C.R., 2000, Isotope stratigraphy of the Ediacaran (Neoproterozoic III) of the Adelaide Rift Complex, Australia, and the overprint of water column stratification: Precambrian Research, v. 100, p. 121-150.

Christie-Blick, N., and Levy, M., 1989, Stratigraphic and tectonic framework of upper Proterozoic and Cambrian rocks in the western United States, *in* Christie-Blick, N., and Levy, M., eds., Late Proterozoic and Cambrian tectonics, sedimentation, and record of Metazoan radiation in the western United States: Washington, D.C., American Geophysical Union, Fieldtrip Guidebook T331, p. 7-21.

Christie-Blick, N., Mount, J.F., Levy, M., Philip W. Signor, and Link, P.K., 1989, Description of stops, *in* Christie-Blick, N., and Levy, M., eds., Late Proterozoic and Cambrian tectonics, sedimentation, and record of Metazoan radiation in the western United States: Washington, D.C., American Geophysical Union, Fieldtrip Guidebook T331, p. 55-113.

Condon, D., Zhu, M., Bowring, S., Wang, W., Yang, A., and Jin, Y., 2005, U-Pb ages from the Neoproterozoic Doushantuo Formation, China: Science, v. 308, p. 95-98.

Corsetti, F.A., and Kaufman, 2003, Stratigraphic investigations of carbon isotope anomalies and Neoproterozoic ice ages in Death Valley, California: Geological Society of America, Bulletin, v.115, p. 916-932.

Corsetti, F.A., and Kaufman, A.J., 2005, The relationship between the Neoproterozoic Noonday Dolomite and the Ibex Formation: new observations and their bearing on 'snowball Earth': Earth-Science Reviews, v. 73, p. 63-78.

Corsetti, F.A., Link, P.K., and Lorentz, N.J., 2007, $\delta^{13}C$ chemostratigraphy of the Neoproterozoic succession near Pocatello, Idaho, U.S.A.: implications for glacial chronology and regional correlations: SEPM Special Publication No. 86, p. 193-205.

Crittenden, M.D., Jr., 1972, Geologic map of the Browns Hole Quadrangle, Utah: U.S. Geological Survey Geologic Quadrangle Map GQ-968, scale 1:24,000, 1 sheet.

Crittenden, M.D., Jr., Calkins, F.C., Sharp, B.J., Baker, A.A., and Bromfield, C.S., 1978, Geology of Big Cottonwood mining district: Utah Geological and Mineral Survey Map 49, scale 1:24,000, 1 sheet.

Crittenden, M.D., Jr., Christie-Blick, N., and Link, P.K., 1983, Evidence for two pulses of glaciation during the late Proterozoic in northern Utah and southeastern Idaho: Geological Society of America Bulletin, v. 94, p. 437-450.

Crittenden, M.D., Jr., Schaeffer, F.E., Trimble, D.E., and Woodward, L.A., 1971, Nomenclature and correlation of some upper Precambrian and basal Cambrian sequences in western Utah and southeastern Idaho: Geological Society of America Bulletin, v. 82, p. 581-602.

Crittenden, M.D., Jr., and Wallace, C.A., 1973, Possible equivalents of the Belt supergroup in Utah, *in* Belt Symposium: Moscow, Idaho, Department of Geology, University of Idaho and Idaho Bureau of Mines and Geology, v. 1, p. 116-138.

Fike, D.A., Grotzinger, J.P., Pratt, L.M., and Summons, R.E., 2006, Oxidation of the Ediacaran ocean: Nature, v. 444, p. 744-747.

Fitton, J.G., and Dunlop, H.M., 1985, The Cameroon line, West Africa, and its bearing on the origin of oceanic and continental alkali basalt: Earth and Planetary Science Letters: v. 72, p. 23-38.

Gill, J.B., 1981, Orogenic andesites and plate tectonics: Springer-Verlag, 390 p.

Halverson, G.P., Hoffman, P.F., Schrag, D.P., Maloof, A.C., and Rice, A.H.N., 2005, Toward a Neoproterozoic composite carbon-isotope record: Geological Society of America Bulletin, v. 117, p. 1181-1207.

Harper, G.D., and Link, P.K., 1986, Geochemistry of Upper Proterozoic rift-related volcanics, northern Utah and southeastern Idaho: Geology, v. 14, p. 864-867.

Hintze, L.F., Willis, G.C., Laes, D.Y.M., Sprinkel, D.A., and Brown, K.D., 2000, Digital Geologic map of Utah: Utah Geological Survey, scale 1:500,000, 2 sheets.

Hoffman, P.F., 1991, Did the breakout of Laurentia turn Gondwanaland inside-out?: Science, v. 252, p. 1409-1412.

Hoffman, P.F., and Schrag, D.P., 2002, The snowball Earth hypothesis: testing the limits of global change: Terra Nova, v. 14, p.129-155.

Housh, T., and Bowring, S.A., 1991, Lead isotopic heterogeneities within alkali feldspars: implications for the determination of initial lead isotopic compositions: Geochemica et Cosmochimica Acta, v. 55, p. 2309-2316.

Johnson, B.R., and Raines, G.L., 1996, Digital representation of the Idaho state geologic map: a contribution to the Interior Columbia River Basin Ecosystem Management Project: U.S. Geological Survey Open-File Report 95-690, 22 p.

Kirschvink, 1980, The least-squares line and plane and the analysis of paleomagnetic data: Geophysical Journal of the Royal Astronomical Society, v. 62, p. 699-218.

Kirschvink, J.L., Mound, J., Mitrovitca, J.X., Raub, T.D., Evans, D.A.D., and Kopp, R.E., 2005, Rapid inertial-interchange true polar wander during Ediacaran time induced by intrusion of the Sept-Îles intrusive suite, Quebec, Canada: a possible trigger for massive sea-level and carbon isotopic excursions: Proceedings of the Gondwana XII conference, Mendoza, Argentina, Nov. 2005.

Kirschvink, J.L., Ripperdan, R.L., and Evans, D., 1997, Evidence for a large-scale reorganization of early Cambrian continental masses by inertial interchange true polar wander: Science, v. 277, p. 541-545.

Knoll, A.H., and Carroll, S.B., 1999, Early animal evolution: emerging views from comparative biology and geology: Science, v. 284, p. 2129-2137.

Le Guerroué, E., Allen, P.A., Cozzi, A., Etienne, J.L., and Fanning, M., 2006, 50 Myr recovery from the largest negative $\delta^{13}C$ excursion in the Ediacaran ocean: Terra Nova, v. 18, p. 147-153.

Le Maitre, R.W., Bateman, D., Dudek, A., and Keller, J., 1989, A classification of igneous rocks and glossary of terms: recommendations of the International Union of Geological Sciences Subcommission on the Systematics of Igneous Rocks: Oxford, Boston, Blackwell, 193 p.

Lorentz, N.J., Corsetti, F.A., and Link, P.K., 2004, Seafloor precipitates and C-isotope stratigraphy from the Neoproterozoic Scout Mountain member of the Pocatello Formation, southeast Idaho: implications for Neoproterozoic earth system behavior: Precambrian Research, v. 130, p. 57-70.

Ojakangas, R.W., and Matsch, C.L., 1980, Upper Precambrian (Eocambrian) Mineral Fork Tillite of Utah: a continental glacial and glaciomarine sequence: Geological Society of America Bulletin, v. 91, p. 495-501.

Petterson, R., Prave, A., Wernicke, B., and Fallick, A.E., 2007, New stratigraphic and isotopic constraints on the Cryogenian-Ediacaran strata of Death Valley region, Geological Society of America Abstracts with Programs, v. 39, no. 6, p. 222.

Prave, A.R., 1999, Two diamictites, two cap carbonates, two $\delta^{13}C$ excursions, two rifts: the Neoproterozoic Kingston Peak Formation, Death Valley, California: Geology, v. 27, p. 339-342.

Rhodes, J.M., 1996, Geochemical stratigraphy of lava flows sampled by the Hawaii Scientific Drilling Project: Journal of Geophysical Research, v. 101, p. 11729-11746.

Rothman, D.H., Hayes, J.M., and Summons R.E., 2003, Dynamics of the Neoproterozoic carbon cycle: Proceedings of the National Academy of Sciences, v. 100, p. 8124-8129.

Smith, L.H., Kaufman, A.J., Knoll, A.H., and Link, P.K., 1994, Chemostratigraphy of predominantly siliciclastic Neoproterozoic successions: a case study of the Pocatello Formation and Lower Brigham Group, Idaho, USA: Geological Magazine, v. 131, p. 301-314.

Sorensen, M.L., and Crittenden, M.D., Jr., 1976, Preliminary geologic map of the Mantua Quadrangle and part of the Willard Quadrangle, Box Elder, Weber, and Cache Counties, Utah: U.S. Geological Survey, Miscellaneous Field Studies Map MF-720, scale 1:24,000.

Stacey, J.S., and Kramers, J.D., 1975, Approximation of terrestrial lead isotope evolution by a two-stage model, Earth and Planetary Science Letters, v. 26, p. 207-221.

Stewart, J.H., 1970, Upper Precambrian and lower Cambrian strata in the southern Great Basin, California and Nevada: U.S. Geological Survey Professional Paper 620, 206 p.

Summa, C.L., 1993, Sedimentologic, stratigraphic, and tectonic controls of a mixed carbonate-siliciclastic succession: Neoproterozoic Johnnie Formation, southeast California [Ph.D. thesis]: Cambridge, Massachusetts Institute of Technology, 332 p.

Sun, S.S., and McDonough, W.F., 1989, Chemical and isotopic systematics of oceanic basalts; implications for mantle composition and processes, *in* Saunders, A.D., and Norry, M.J., eds., Magmatism in the oceanic basins: Geological Society of London Spec. Pub. 42, p. 313-345.

FIGURE CAPTIONS

Figure 1. Shaded relief map of northern Utah and southern Idaho showing distribution of Neoproterozoic sediments. Geology of Utah and Idaho after Hintze et al. (2000) and Johnson and Raines (1996), respectively.

Figure 2. Part of the Late Proterozoic to Cambrian stratigraphy of the Browns Hole Quadrangle (Crittenden, 1972) and stratigraphic positions of samples discussed in text.

Figure 3. Geologic map of the Browns Hole quadrangle (Crittenden, 1972) showing sample locations. Abbreviations: pCga-Maple Canyon Fm., pCk-Kelley Canyon Fm., pCc-Caddy Canyon Quatzite, pCi-Inkom Fm., pCm-Mutual Fm., pCb-Volcanic member of the Browns Hole Fm., pCt-Terra Cotta member of the Browns Hole Fm., CpCgl-Lower member of the Geertsen Canyon Quartzite, CpCgu-Upper member of the Geertsen Canyon Quartzite, TKwe-Cretaceous to Eocene Wasatch and Evanston Fms., Qal-Quaternary alluvium.

Figure 4. Geochemical data from the Browns Hole basalt. (A) Primitive mantle normalized trace element diagram. Oceanic island basalt (OIB) and primitive mantle compositions from Sun and McDonough (1989). (B) Total alkali-silica diagram.

Figure 5. U-Pb concordia diagram for Browns Hole basalt apatites. Multi-grain analyses shown as filled ellipses.

Figure 6. Paleomagnetic data from the Browns Hole quadrangle. (A) Vector component, equal area, and magnetic intensity (J/J_0) diagrams for sample SF5 from the volcanic member of the Browns Hole Fm. in the south limb of the fold. The only magnetic component discernable from this sample is parallel to the present-local magnetic field (PLF), marked by a star at the center of the cluster of data points. The PLF component vector is drawn as a blue arrow in this and subsequent plots. D=declination; I=inclination. (B) Equal area plot showing the orientations of all PLF components as well as the mean inclination and declination of these individual measurements. (C) Summary of data for sample MF10 from the Browns Hole basalt in the north limb of the fold. This sample displays evidence for two magnetic components: a low-temperature PLF component that dominates the NRM, and a higher temperature, high-inclination B component that trends to the NW in both geographic and tilt-corrected coordinates. Note that the magnetic intensity (J_0) of this sample (the only basalt sample shown on the figure) is ~1000x greater than the other samples. On this and subsequent plots, the B vector is shown as a green arrow. (D) Data for sample MF19 from the Inkom Fm. in the south limb of the fold. This sample also shows evidence for both PLF and a high-inclination B component. The B components from this sample (south limb) and MF10 (north limb, panel C) plot in similar locations on geographic equal area plots but in different locations on tilt-corrected plots, suggesting that the B component was acquired after folding. (E) All measured B components plotted in geographic coordinates. Note that orientations from samples in both limbs overlap. (F) B components plotted in tilt-corrected coordinates. On this plot, the orientations from either limb diverge, providing strong evidence that the B component fails a fold test, i.e., the B component was acquired

after folding. (G) Data for sample MF4 from the upper Mutual Fm. in the north limb of the fold. The lowest temperature component identifiable from the data is the high-inclination B component. Note the similarity with the B component from sample MF10 (also from the north limb, panel C). In addition to the B component, there is evidence for a higher temperature, low-inclination C component. On this and the following plot, the C vector is shown as a purple arrow. (H) Data for sample SF12 from the Mutual Fm. in the south limb of the fold. This sample also has evidence for the B and C components. Taken together, the data from this sample and MF4 (panel G) suggest that the C component trends SW-NE and plunges slightly to the SW.

Figure 7. Existing C isotope data from Neoproterozoic carbonates in northern Utah and southern Idaho. Lithostratigraphy after Christie-Blick et al. (1989) and Corsetti et al. (1987) based on thicknesses near Pocatello. Datum is top of the upper diamictite of the Pocatello Fm. (Smith et al., 1994).

Figure 1

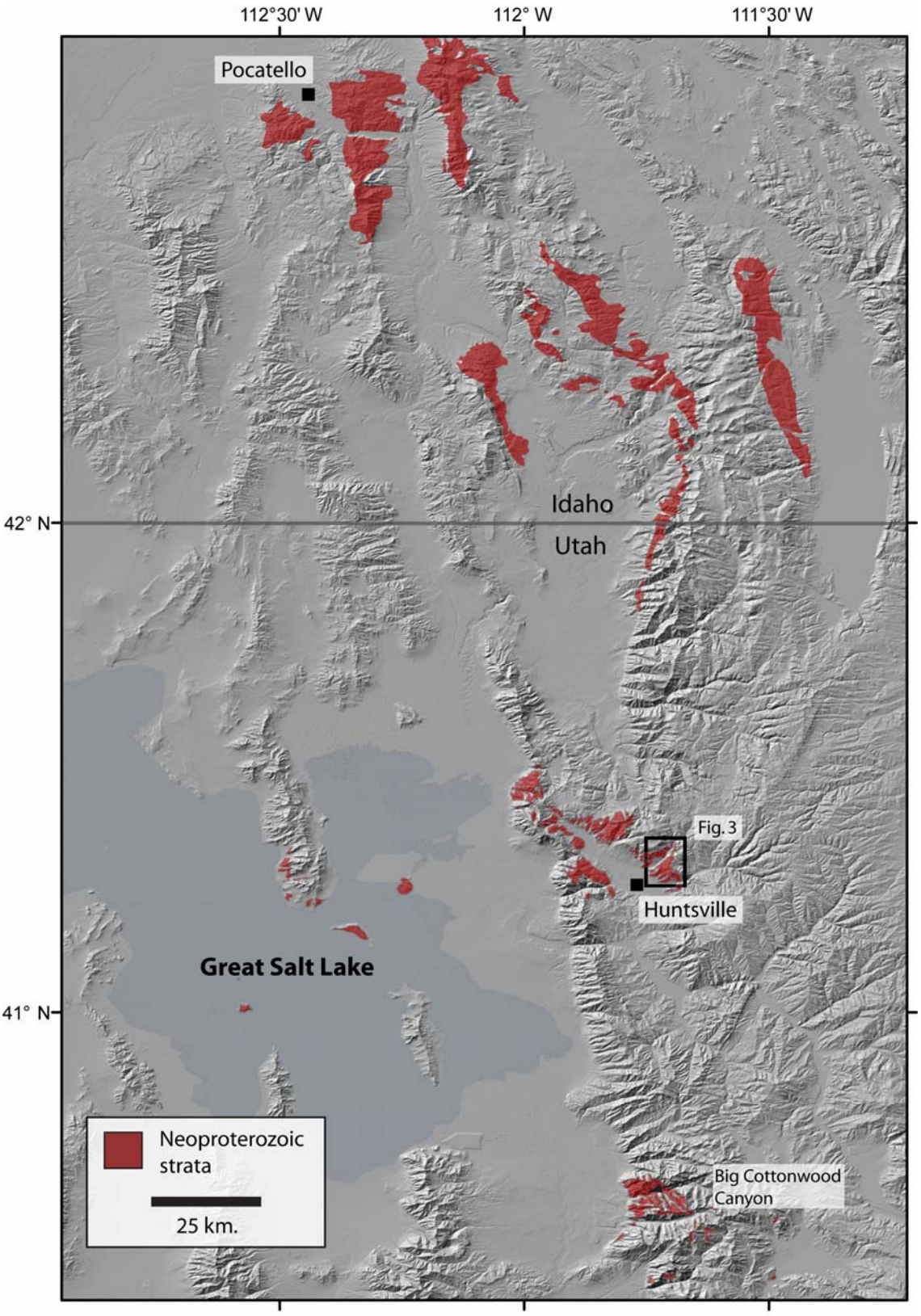
112°30' W
112° W
111°30' W
Pocatello
Idaho
Utah
42° N
41° N
Fig. 3
Huntsville
Great Salt Lake
Big Cottonwood Canyon
Neoproterozoic strata
25 km.

Figure 2

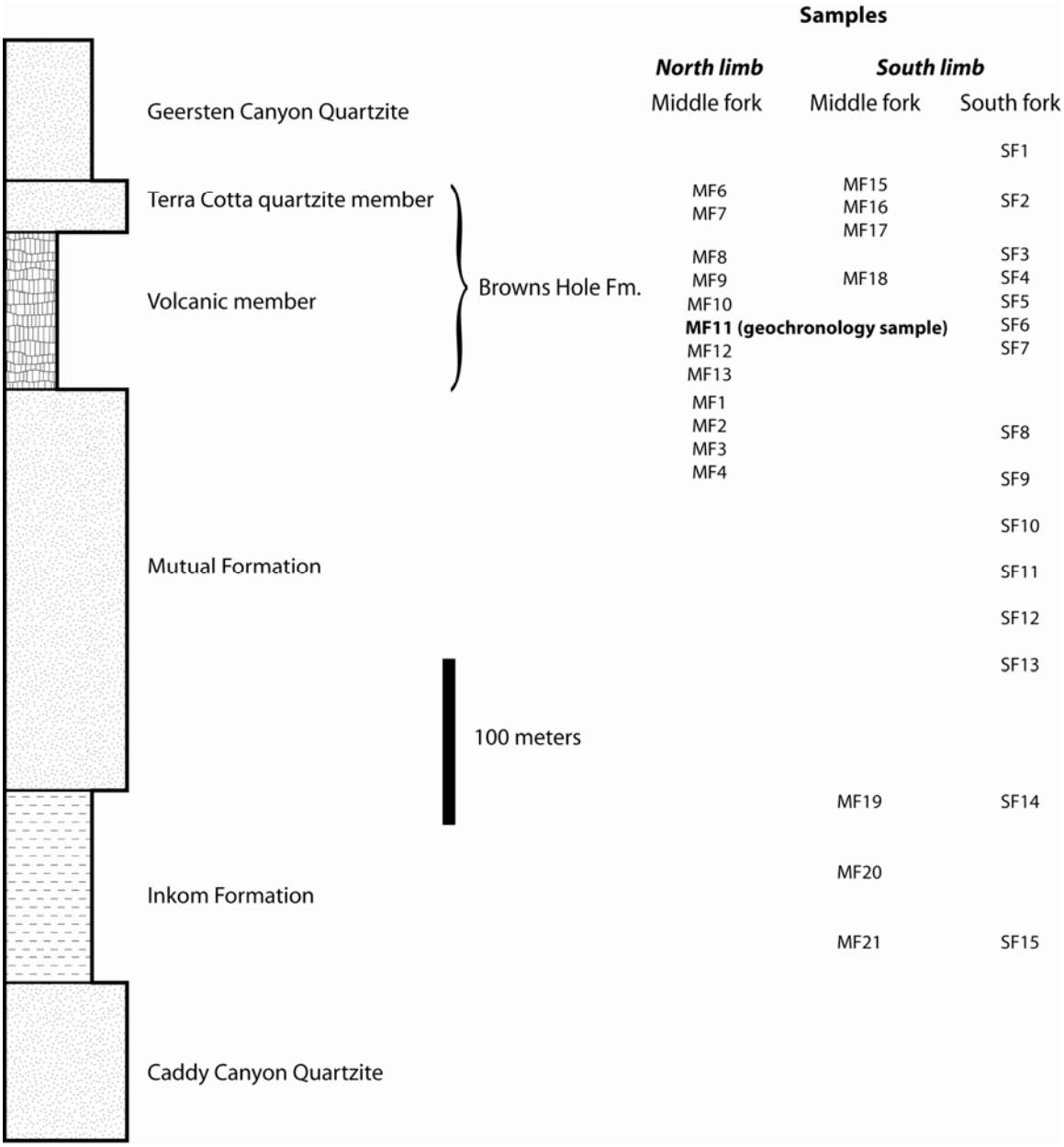
Samples
North limb
South limb
Middle fork
Middle fork
South fork
Geersten Canyon Quartzite
Terra Cotta quartzite member
Volcanic member
Browns Hole Fm.
Mutual Formation
Inkom Formation
Caddy Canyon Quartzite
100 meters
MF6
MF7
MF8
MF9
MF10
MF11 (geochronology sample)
MF12
MF13
MF1
MF2
MF3
MF4
MF15
MF16
MF17
MF18
MF19
MF20
MF21
SF1
SF2
SF3
SF4
SF5
SF6
SF7
SF8
SF9
SF10
SF11
SF12
SF13
SF14
SF15

Figure 3

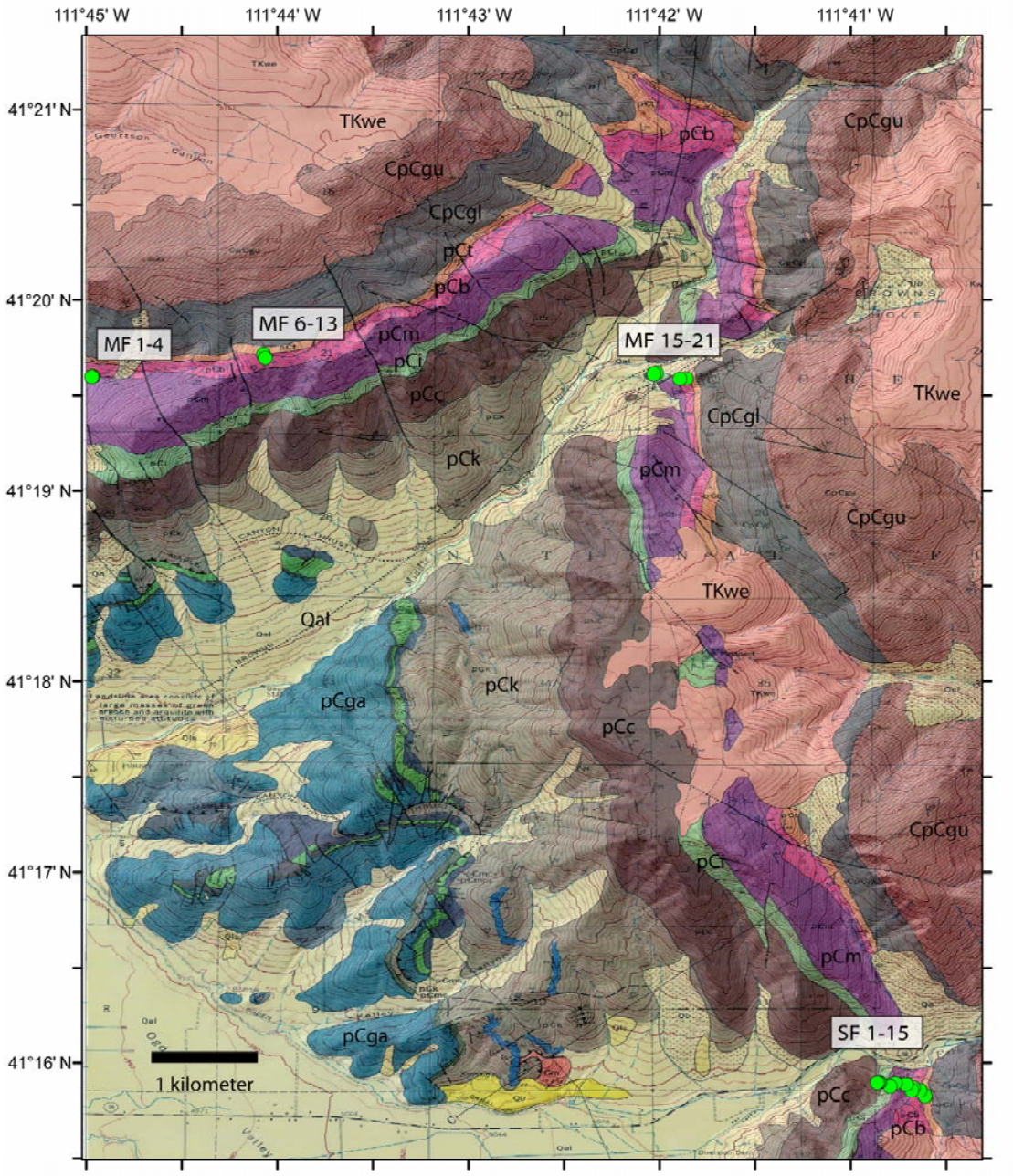
111°45' W
111°44' W
111°43' W
111°42' W
111°41' W
41°21' N
41°20' N
41°19' N
41°18' N
41°17' N
41°16' N
TKwe
CpCgu
CpCgl
pCt
pCb
pCm
pCi
pCc
pCk
pCga
Qal
MF 1-4
MF 6-13
MF 15-21
SF 1-15
1 kilometer

Figure 4

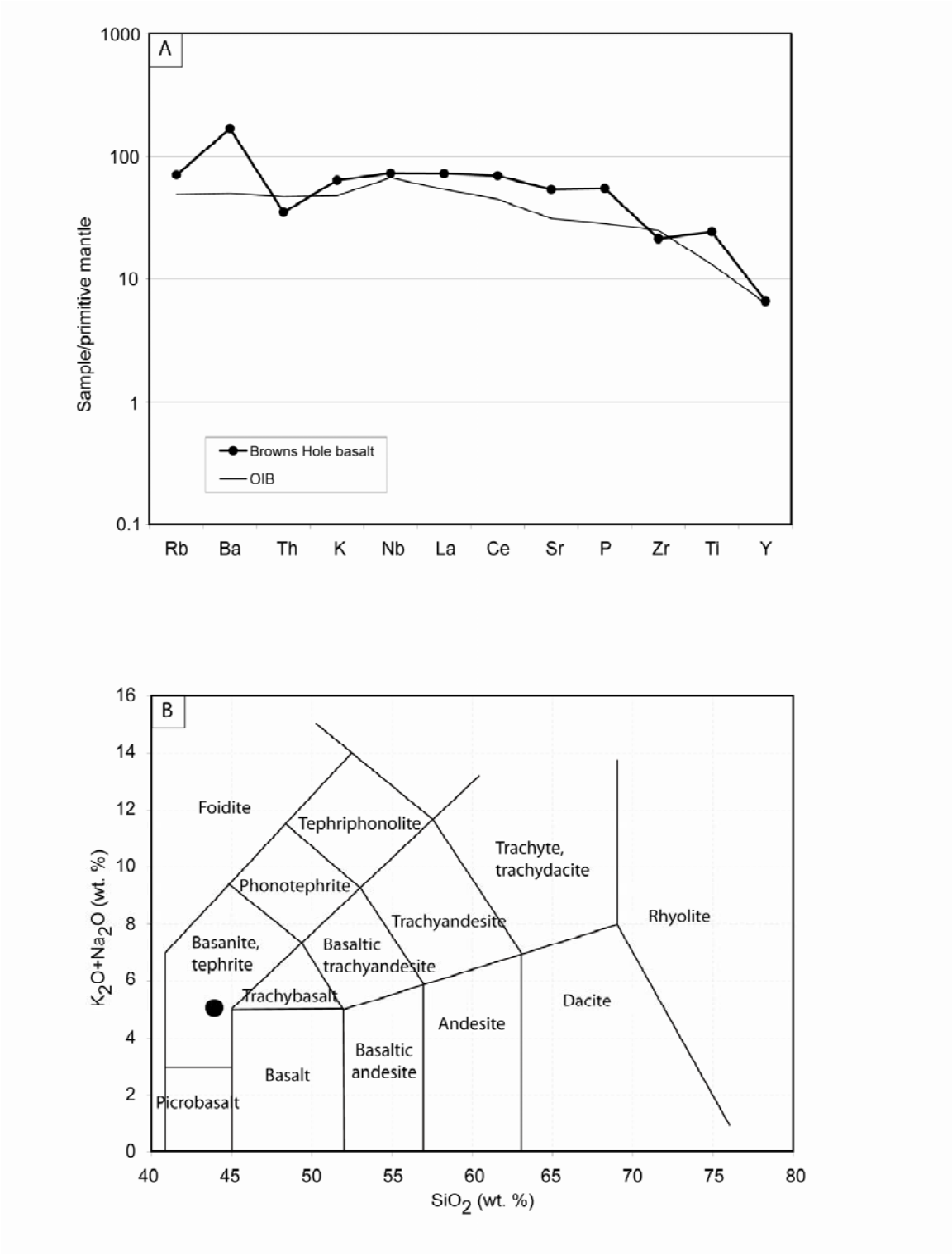
A
1000
100
10
1
0.1
Sample/primitive mantle
Browns Hole basalt
OIB
Rb
Ba
Th
K
Nb
La
Ce
Sr
P
Zr
Ti
Y
B
16
14
12
10
8
6
4
2
0
K_2O+Na_2O (wt. %)
Foidite
Tephriphonolite
Phonotephrite
Trachyte, trachydacite
Trachyandesite
Rhyolite
Basanite, tephrite
Basaltic trachyandesite
Trachybasalt
Andesite
Dacite
Basaltic andesite
Basalt
Picrobasalt
40
45
50
55
60
65
70
75
80
SiO_2 (wt. %)

Figure 5

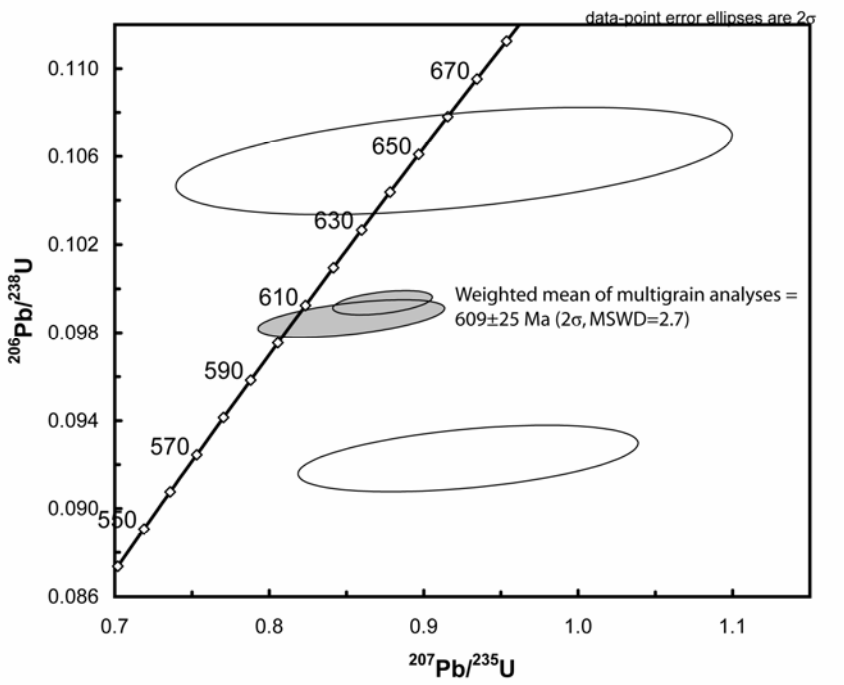
data-point error ellipses are 2σ
0.110
0.106
0.102
0.098
0.094
0.090
0.086
0.7
0.8
0.9
1.0
1.1
$^{206}Pb/^{238}U$
$^{207}Pb/^{235}U$
670
650
630
610
590
570
550
Weighted mean of multigrain analyses =
609±25 Ma (2σ, MSWD=2.7)

Figure 6

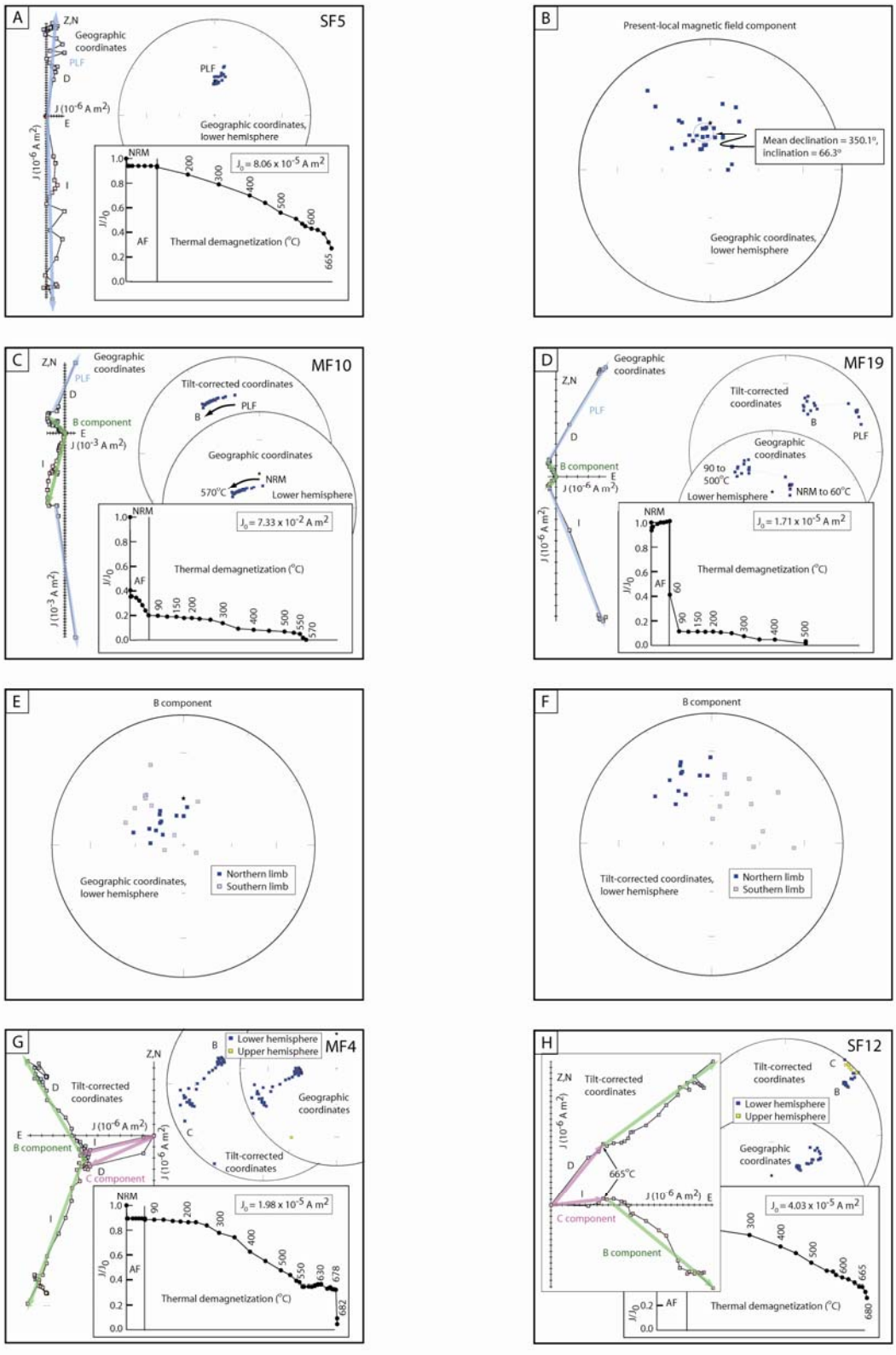
A
SF5
Z,N
Geographic coordinates
PLF
D
J (10-6 A m2)
E
I
Geographic coordinates, lower hemisphere
NRM
J0 = 8.06 x 10-5 A m2
J/J0
AF
Thermal demagnetization (°C)
B
Present-local magnetic field component
Mean declination = 350.1°, inclination = 66.3°
Geographic coordinates, lower hemisphere
C
MF10
Tilt-corrected coordinates
B component
J (10-3 A m2)
570°C
Lower hemisphere
J0 = 7.33 x 10-2 A m2
D
MF19
90 to 500°C
NRM to 60°C
J0 = 1.71 x 10-5 A m2
E
B component
Northern limb
Southern limb
F
Tilt-corrected coordinates, lower hemisphere
G
MF4
Lower hemisphere
Upper hemisphere
C component
J0 = 1.98 x 10-5 A m2
H
SF12
665°C
J0 = 4.03 x 10-5 A m2

Figure 7

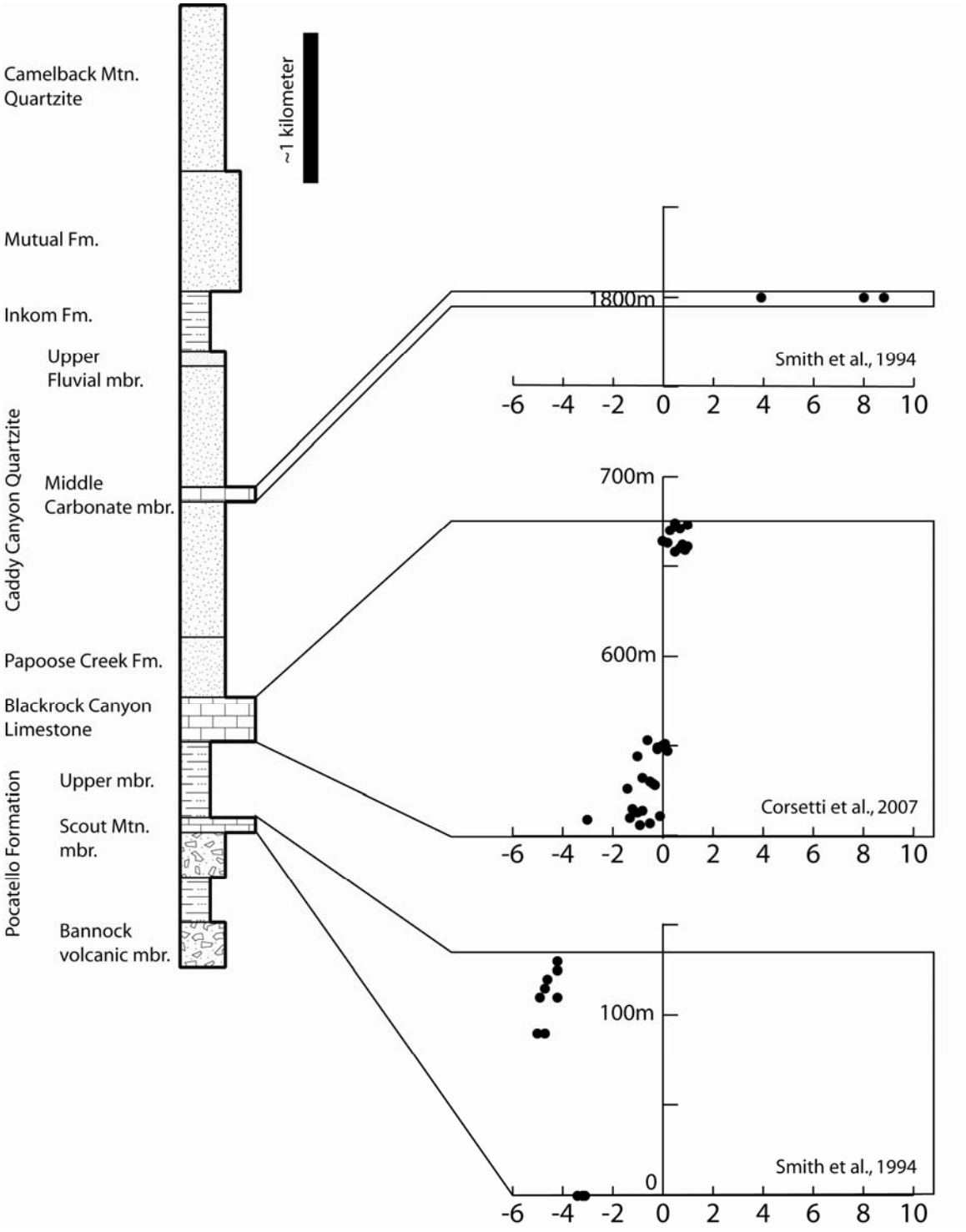
Camelback Mtn. Quartzite
~1 kilometer
Mutual Fm.
Inkom Fm.
Upper Fluvial mbr.
Middle Carbonate mbr.
Caddy Canyon Quartzite
Papoose Creek Fm.
Blackrock Canyon Limestone
Upper mbr.
Scout Mtn. mbr.
Pocatello Formation
Bannock volcanic mbr.
1800m
Smith et al., 1994
700m
600m
Corsetti et al., 2007
100m
0
Smith et al., 1994
-6 -4 -2 0 2 4 6 8 10

TABLE 1: XRF major and trace element data from the Browns Hole basalt

SiO_2 (%)	43.53
TiO_2 (%)	5.26
Al_2O_3 (%)	14.10
Fe_2O_3 (%)	14.99
MnO (%)	0.42
MgO (%)	6.09
CaO (%)	9.17
Na_2O (%)	3.08
K_2O (%)	1.93
P_2O_5 (%)	1.20
Total (%)	99.77
Rb (ppm)	45
Ba (ppm)	1181
Th (ppm)	3
Nb (ppm)	52
La (ppm)	50
Ce (ppm)	124
Sr (ppm)	1138
P (ppm)	5217
Zr (ppm)	240
Y (ppm)	30
Cr (ppm)	33
Ni (ppm)	38

TABLE 2: U-Pb geochronology of the Browns Hole basalt

Apatite U-Pb data

						Concentrations				Ratios						Age (Ma)			
Sample/ Fractions	Number of grains	Wt. (µg) (a)	Pb(c) (pg) (b)	Pb*/ Pb(c)	Th/U	U (ppm)	Pb (ppm)	$^{206}Pb/^{204}Pb$ (c)	$^{208}Pb/^{206}Pb$ (d)	$^{206}Pb/^{238}U$ (e)	err (2σ%)	$^{207}Pb/^{235}U$	err (2σ%)	$^{207}Pb/^{206}Pb$	err (2σ%)	$^{206}Pb/^{238}U$	$^{207}Pb/^{235}U$	$^{207}Pb/^{206}Pb$	Corr. coef.
CVMF11	apatite																		
a1	1	3.7	1.5	0.3	3.591	0.64	0.30	28.30	1.220	0.105784	(1.90)	0.91900	(16.14)	0.06301	(15.33)	**648.21**	**661.83**	**708.5**	0.473
a2	1	3.6	1.6	0.5	2.355	1.08	0.39	32.36	1.326	0.09215	(1.35)	0.92813	(9.76)	0.07305	(9.21)	**568.24**	**666.65**	**1015.3**	0.461
a3	5	7.9	2.7	0.8	3.568	1.40	0.51	42.62	1.280	0.098576	(.71)	0.85194	(5.83)	0.06268	(5.47)	**606.06**	**625.71**	**697.4**	0.549
a4	8	12.6	3.3	1.0	3.344	1.25	0.44	47.45	1.251	0.09930	(.47)	0.87221	(3.04)	0.06370	(2.85)	**610.31**	**636.76**	**731.8**	0.456

Weighted mean of a3 and a4 = <u>609±25 Ma (2σ)</u>, MSWD = 2.7, probability = 0.10

(a) Sample weights are estimated from grain images.
(b) Total common-Pb in analyses.
(c) Measured ratio corrected for spike and fractionation only.
(d) Radiogenic Pb.
(e) Corrected for fractionation, spike, blank, and initial common Pb.

Mass fractionation correction of 0.25%/amu ± 0.04%/amu (atomic mass unit) was applied to single-collector Daly analyses and 0.07%/amu ± 0.04% for dynamic Faraday-Daly analyses. Total procedural blank less than 0.3 pg for Pb and less than 0.1 pg for U.

Blank isotopic composition: $^{206}Pb/^{204}Pb = 18.27 \pm 0.1$, $^{207}Pb/^{204}Pb = 15.59 \pm 0.1$, $^{208}Pb/^{204}Pb = 38.12 \pm 0.1$.
Corr. coef. = correlation coefficient.
Age calculations are based on the decay constants of Steiger and Jäger (1977).
Common-Pb corrections were calculated by using the model of Stacey and Kramers (1975) and the interpreted age of the sample.

References:
1. Stacey, J.S. and Kramers, J.D., Earth and Planetary Science Letters 26, 207, 1975.
2. Steiger, R.H., and Jäger, E., Earth Planetary Science Letters 36, 359, 1977.

TABLE 2 (continued): U-Pb geochronology of the Browns Hole basalt

Plagioclase step leaching results.
Common Pb composition from step 2 used in subsequent calculations.

Step	Reagent	$^{206}Pb/^{204}Pb$	2σ abs. error	$^{207}Pb/^{204}Pb$	2σ abs. error	$^{208}Pb/^{204}Pb$	2σ abs. error
1	12N HCl	19.4722	0.0052	15.7771	0.0045	37.302	0.012
2	conc. HF 1	17.4701	0.0084	15.4989	0.0075	37.266	0.018
3	conc. HF 2	17.9631	0.0056	15.5572	0.0058	37.670	0.014
	SRM 981*	16.9418	0.0006	15.5000	0.0006	36.727	0.002

* Baker et al. (2004) Chem Geol 211, p.275-303